in silico Plants, 2024, **6**, diae015
https://doi.org/10.1093/insilicoplants/diae015
Advance access publication 30 August 2024
Original Research

Original Research

Model-based inference of a dual role for HOPS in regulating guard cell vacuole fusion

Charles Hodgens[1], DT Flaherty[2], Anne-Marie Pullen[3], Imran Khan[3], Nolan J. English[4], Lydia Gillan[5], Marcela Rojas-Pierce[3] and Belinda S. Akpa[*,1,2,4]

[1]Department of Chemical and Biomolecular Engineering, University of Tennessee-Knoxville, Knoxville, TN 37996, USA
[2]Department of Molecular Biomedical Sciences, North Carolina State University, Raleigh, NC 27607, USA
[3]Department of Plant and Microbial Biology, North Carolina State University, Raleigh, NC 27695, USA
[4]Biosciences Division, Oak Ridge National Laboratory, Oak Ridge, TN 37830, USA
[5]Department of Chemical and Biomolecular Engineering, North Carolina State University, Raleigh, NC 27695, USA

[*]Corresponding author's e-mail address: bakpa1@utk.edu

Handling Editor: Xin-Guang Zhu

Abstract. Guard cell movements depend, in part, on the remodelling of vacuoles from a highly fragmented state to a fused morphology during stomata opening. Indeed, full opening of plant stomata requires vacuole fusion to occur. Fusion of vacuole membranes is a highly conserved process in eukaryotes, with key roles played by two multi-subunit complexes: HOPS (homotypic fusion and vacuolar protein sorting) and SNARE (soluble NSF attachment protein receptor). HOPS is a vacuole tethering factor that is thought to chaperone SNAREs from apposing vacuole membranes into a fusion-competent complex capable of rearranging membranes. In plants, recruitment of HOPS subunits to the tonoplast has been shown to require the presence of the phosphoinositide phosphatidylinositol 3-phosphate. However, chemically depleting this lipid induces vacuole fusion. To resolve this counter-intuitive observation regarding the role of HOPS in regulating plant vacuole morphology, we defined a quantitative model of vacuole fusion dynamics and used it to generate testable predictions about HOPS-SNARE interactions. We derived our model by using simulation-based inference to integrate prior knowledge about molecular interactions with limited, qualitative observations of emergent vacuole phenotypes. By constraining the model parameters to yield the emergent outcomes observed for stoma opening—as induced by two distinct chemical treatments—we predicted a dual role for HOPS and identified a stalled form of the SNARE complex that differs from phenomena reported in yeast. We predict that HOPS has contradictory actions at different points in the fusion signalling pathway, promoting the formation of SNARE complexes, but limiting their activity.

KEYWORDS: Approximate Bayesian computation; parameter estimation; stomata; systems biology; vacuole fusion.

1. INTRODUCTION

Stomata are critical for gas exchange—as required for photosynthesis and the control of leaf transpiration and temperature. Stomatal movement (opening and closing) is tightly controlled in response to exogenous cues such as changes in light or temperature and endogenous cues such as circadian regulation or hormone signalling (Hetherington and Woodward 2003). The transition from closed to open stomata is a complex process with several well-studied component phenomena, including the activation of blue-light photoreceptors, K+ ion influx and water uptake (Kwak *et al.* 2008). Studies by confocal and electron microscopy have shown dynamic changes in the morphology of the vacuole between closed and open stomata (Gao *et al.* 2005, 2009). Specifically, in the closed state of the stoma, the vacuoles within guard cells exhibit a fragmented or highly convoluted morphology, appearing sometimes as numerous small organelles (Gao *et al.* 2005, 2009; Zheng *et al.* 2014; Cao *et al.* 2022). When the pore is open, these same cells exhibit a vacuole morphology typical of other mature plant cells—namely a single large vacuole, or few vacuoles, occupying most of the intracellular space. Importantly, vacuole membrane fusion is necessary for full opening of the pore (Zheng *et al.* 2014).

Fusion of vacuole membranes is a highly conserved process in eukaryotes and is best described in yeast (Chen and Scheller 2001; Wickner 2010). Two multi-subunit protein complexes act in concert to induce vacuole fusion: the homotypic fusion and vacuolar protein sorting (HOPS) complex and soluble NSF attachment protein receptor (SNARE). HOPS is a tethering complex that is recruited from the cytosol by active

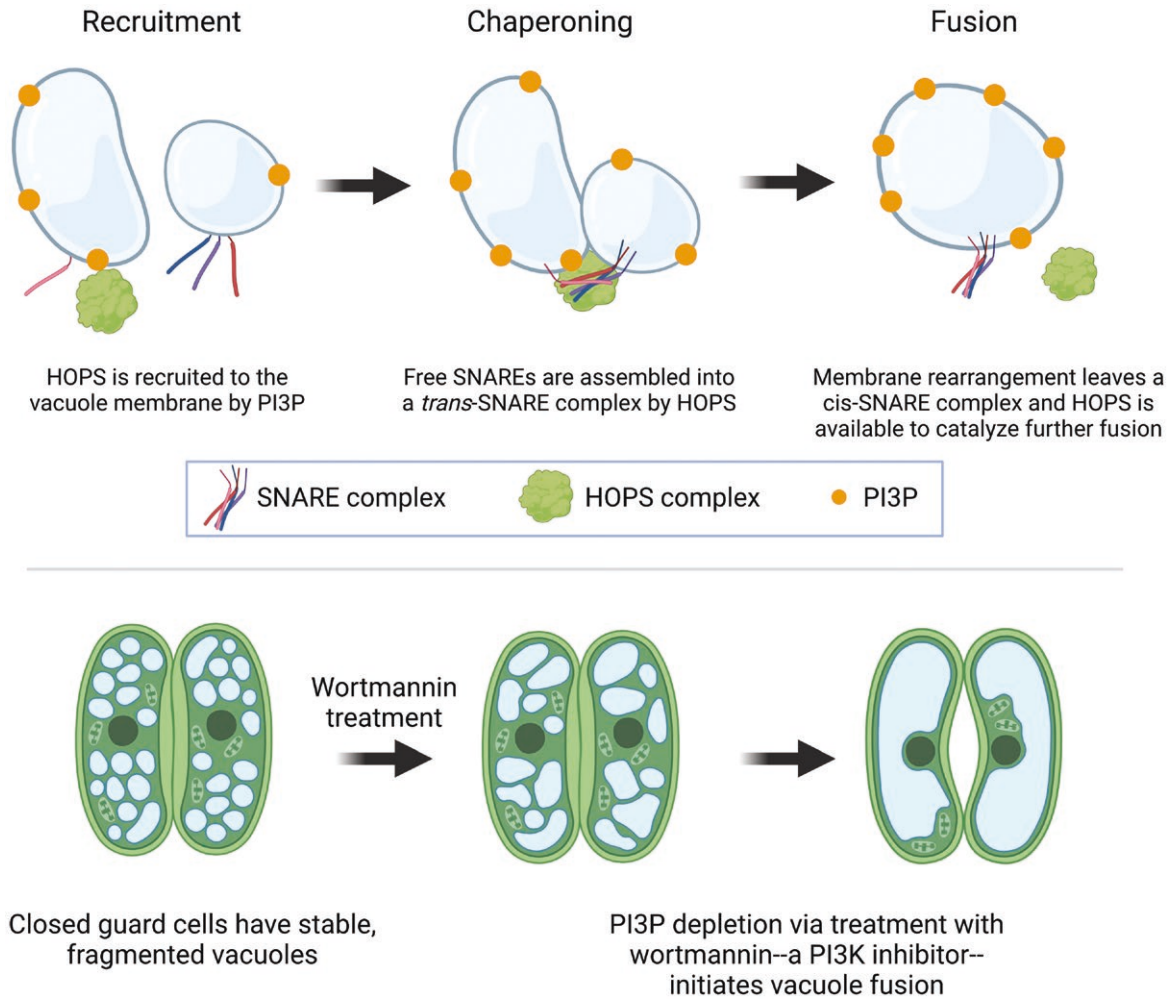

Figure 1. Contradictory results regarding the mode of action of HOPS and PI3P in plant vacuole fusion. (A) HOPS is recruited from a cytosolic pool to the vacuole membrane, due, in part, to the presence of the phosphoinositide PI3P. HOPS is responsible for tethering vacuoles together and chaperoning membrane-embedded SNARE proteins into a *trans*-SNARE fusion complex. Vacuole fusion is mediated by the zippering activity of the SNARE complex. As part of the fusion event, HOPS leaves the membrane. Based on this prior knowledge, one would expect fusion to be impossible in the absence of PI3P. (B) When wortmannin, a PI3K inhibitor, is used to deplete PI3P from the guard cells of a closed stoma, small vacuoles rapidly fuse.

RAB proteins and the presence of specific phosphoinositides at the vacuole membrane (Wickner 2010). HOPS then is thought to provide binding sites for SNAREs from apposing membranes and thereby promote the formation of gap-spanning *trans*-SNARE complexes to support fusion. HOPS was also proposed to proofread the fidelity of the *trans*-SNARE complex and protect it from disassembly (Starai *et al.* 2008; Xu *et al.* 2010). In the case of plant vacuoles, RAB7 has been implicated in homotypic vacuole fusion upstream of HOPS recruitment (Takemoto *et al.* 2018), which also requires the accumulation of phosphatidylinositol 3-phosphate (PI3P) (Brillada *et al.* 2018).

Thus, the series of events leading to plant vacuole fusion, an essential transformation for full opening of the stomata, would seem to be: (1) HOPS subunits arrive at the vacuole membrane, mediated, in part, by the presence of PI3P; (2) HOPS tethers a pair of vacuoles and chaperones their SNARE proteins into the *trans*-SNARE fusion machinery; (3) the *trans*-SNARE complex zippers, exerting the force required to fuse apposing membranes, an event that is accompanied by HOPS release from the membrane (Fig. 1A). Linear logic would lead one to expect that withdrawing PI3P from this system would impair the cell's ability to respond to pore-opening signals by fusing vacuoles. However, depleting PI3P by treating guard cells with the phosphatidyl-inositol 3-kinase (PI3K) inhibitor wortmannin causes spontaneous fusion in plants (Fig. 1B). That is, even in the absence of the appropriate environmental or biological cue, guard cell vacuoles fuse when PI3P, a membrane lipid thought to be required for forming the fusion machinery, is removed (Zheng *et al.* 2014). This seems to be a plant-specific process, as PI3P depletion does not induce vacuole or lysosome fusion in yeast or animal cells (Reaves *et al.* 1996; Boeddinghaus *et al.* 2002; Bright *et al.* 2008).

These observations present a puzzle as to the preconditions for vacuole fusion. To reconcile our prior knowledge with this potentially plant-specific phenomenon, we developed a novel systems model of known and hypothetical events that may control fusion complex assembly and activation

in *Arabidopsis*. Our model consists of ordinary differential equations (ODEs) describing the dynamic recruitment, complexation and interaction of HOPS and SNARE proteins at vacuolar membranes. We used mass action kinetics to capture the dependence of each event on the abundance of required species. While models of this type can offer a machine-assisted approach to reasoning about biological data, one typically desires abundant, quantitative data to inform such models. However, biological data often come in the form reported in Fig. 2, which captures emergent, qualitative vacuole phenotypes. Directly measuring the kinetics of individual molecular-scale events is challenging. In addition, these data do not offer a finely resolved time course of stomatal dynamics or vacuole number. In principle, one could derive quantitative information about vacuole size and number from live-cell images. That would require (i) a sufficient number of images to obtain statistically sound estimates, (ii) automated image segmentation algorithms to alleviate the laborious tasks of counting and measuring vacuoles, (iii) images of sufficient quality for successful application of such algorithms and (iv) adequate financial and skilled human resources to perform the larger number of experiments required.

In lieu of immediately committing significant resources to gather quantitative data, we sought to inform the kinetics of molecular events by simulation-based inference (Johnston *et al.* 2014; Ross *et al.* 2017; Cheng and Kirkpatrick 2019; Järvenpää *et al.* 2019; Ziegler*et al.* 2019; Carballo-Pacheco *et al.* 2020) using qualitative observations (Fig. 2). Essentially, knowing what system perturbations should promote fusion, and having some sense of how fusion rates differ under different perturbations, we can classify candidate parameter sets as plausible or implausible based on the model's ability to predict the expected fusion dynamics. This means that we make no pretense of defining a single parameterization, but instead computationally pre-screen the model to exclude kinetics that are inconsistent with current knowledge and define the domain of kinetics that is worthy of further interrogation. We sought to determine whether this information might be adequate to constrain our definition of plausible biological mechanisms via a mathematical model. If so, such a modelling approach could pre-screen likely regulatory mechanisms and inform a targeted experimental strategy in which to invest greater time and resources.

There have been prior modelling efforts in the general area of stomatal opening. Their focus has been on signalling events upstream of vacuole remodelling (e.g. from photoreceptor activation to water uptake and ion-channel fluxes) (Hills *et al.* 2012; Albert *et al.* 2017). There have also been biomechanical models capturing the impact of the opening process on cell shape and stoma aperture (Carter *et al.* 2017; Vialet-Chabrand *et al.* 2017; Woolfenden *et al.* 2017). Our model is the first to address the molecular processes regulating organelle remodelling—a phenomenon required for upstream signalling to be transduced to full opening of the pore. Furthermore, we shed light on plant-specific elements of this phenomenon, which share many conserved features in common with yeast vacuole. The observation that depleting PI3P induces fusion forced us to reconsider how the reductionist prior knowledge about interactions amongst HOPS, PI3P and SNARES fits together to produce the emergent biological phenomenon of vacuole remodelling. Formally interrogating our qualitative observations through the lens of a model allowed us to put forward a systems-level definition of the role of HOPS. Specifically, we posit that HOPS acts as both a facilitator and inhibitor of vacuole fusion, executing each role at a different point in the non-linear dynamic system regulating SNARE complex formation and activation.

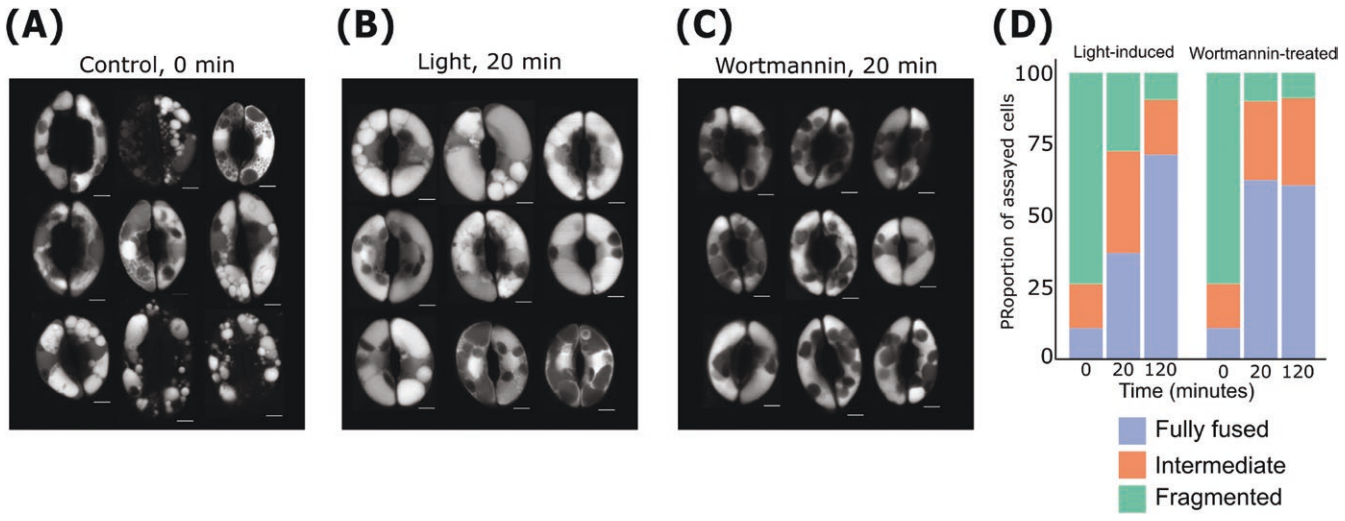

Figure 2. Fusion due to wortmannin treatment proceeds more quickly than fusion due to a fusicoccin stimulus. (A) Dark-acclimated, ABA-treated *Arabidopsis thaliana* guard cells were imaged prior to treatment with a fusion-inducing stimulus. (B) Vacuole morphology after 20 min of fusicoccin and light treatment and (C) after 20 min of wortmannin treatment. (D) A qualitative survey of vacuole morphology reveals rapid wortmannin-driven fusion. We classified guard cells as having fragmented, fully fused or intermediate vacuole phenotypes at 0 min, 20 min, and 2 h after inducing fusion. The evolution of vacuole morphology was complete after 20 min in the wortmannin-treated cell group. Vacuole morphology in fusicoccin-treated cells continued to evolve after that time. Vacuoles were stained with BCECF. Chloroplasts (dark ovals inside guard cells) typically do not take up the vacuole stain. Source data for panel D available in Supplemental Table 1.

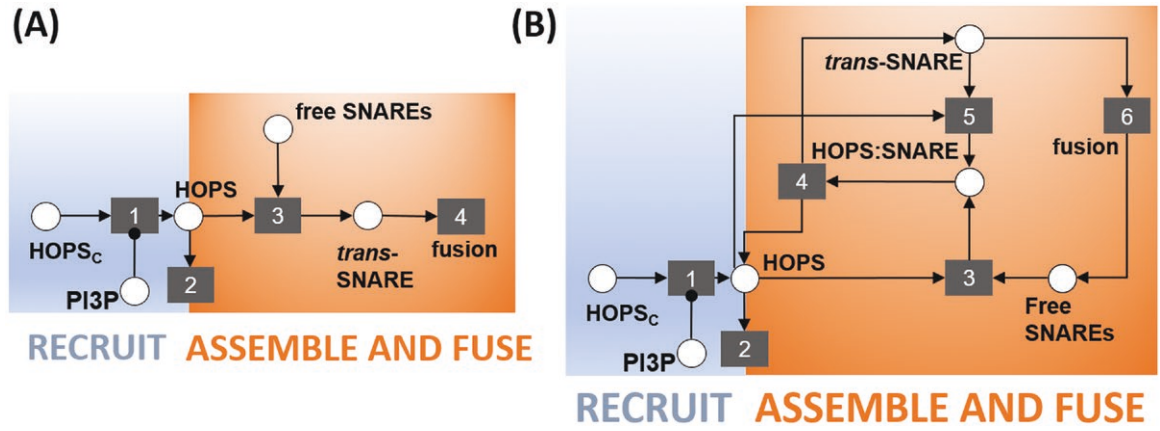

Figure 3. Two schematics of increasing complexity describe potential molecular events leading to vacuole fusion. (A) A schematic of the known signalling events leading to vacuole fusion. Circles represent species and their complexes. Squares represent events. Arrows into an event indicate the logical requirements for that event to take place. Arrows originating from an event indicate the event's consequences. The replacement of an arrowhead by a dot indicates that a species is required for an event to take place, but that species is not consumed when the event happens. Thus, PI3P is required for HOPS to be recruited from the cytosol to the membrane (event 1). HOPS may then leave the membrane (event 2) or participate in chaperoning of free SNARE proteins into a *trans*-SNARE complex (event 3). Finally, the *trans*-SNARE complex drives fusion activity (event 4). This linear scheme and its cascading series of logical requirements implies that the removal of PI3P can only prevent fusion. (B) Schematic of increased complexity positing the spontaneous dissociation (and reassociation) of a HOPS:*trans*-SNARE super-complex. Events 1 and 2 are retained from part A. HOPS chaperoning of free SNARES (event 3) results in a HOPS:*trans*-SNARE super-complex from which HOPS must be removed—if we assume that the *trans*-SNARE complex is the competent species driving fusion (event 6). The simplest way we can posit for HOPS to be removed is by spontaneous dissociation (event 4). Species that dissociate spontaneously can likely reassociate (event 5).

2. RESULTS AND DISCUSSION

2.1 PI3P depletion causes vacuoles to fuse faster than fusicoccin treatment does

Stoma vacuole fusion can be induced under laboratory conditions by treatment with fusicoccin or wortmannin. Fusicoccin is a fungal toxin that promotes stomata opening by activation of the plasma membrane H^+ ATPase (Assmann and Schwartz 1992; Shimazaki *et al.* 2007). Thus, fusicoccin can be used as a proxy for the signalling pathway that triggers stomata opening downstream of light perception (Shimazaki *et al.* 2007), but fusicoccin is not expected to drive vacuole fusion directly. The modelling strategy we report herein was motivated by experiments comparing the dynamics of fusicoccin- and wortmannin-induced vacuole fusion. We first induced stomata closure by incubating leaves with abscisic acid (ABA) in the dark. Consistent with prior results (Zheng *et al.* 2014; Hsu *et al.* 2021), this resulted in guard cells with highly fragmented vacuoles (Fig. 2A). The leaves were subsequently treated with either fusicoccin or wortmannin, and both treatments induced vacuole fusion (Fig. 2B and C, respectively).

Vacuoles in wortmannin-treated guard cells fused rapidly, completing this change in morphology within 20 min (Fig. 2D, left). At that 20-min timepoint, vacuoles fusing in response to fusicoccin still presented an intermediate morphology, with fusion activity continuing for over an hour (Fig. 2D, right). Thus, guard cell vacuole fusion presents non-heuristic emergent dynamics. Specifically, (1) wortmannin depletes PI3P from vacuole membranes, and thereby initiates a series of events previously thought to depend on the presence of that lipid, and (2) the fusion process initiated by wortmannin treatment is accelerated compared to that associated with normal physiological responses (mimicked here by fusicoccin treatment). With the goal of proposing a molecular pathway capable of explaining these observations, we used mathematical modelling as a tool to integrate these phenotypic observations with prior knowledge about the molecular machinery of fusion.

2.2 Prior knowledge of molecular mechanisms fails to explain PI3P regulation of fusion

By collating information about membrane fusion in plants, yeast and animal cells, we established the following as prior knowledge about the molecular events leading to vacuole fusion: (1) Membrane fusion requires a *trans*-SNARE complex (Ungermann *et al.* 1998); (2) HOPS chaperones free SNARE proteins into a *trans*-SNARE complex (Mima *et al.* 2008; Zick and Wickner 2013); (3) The HOPS subunit VPS41 (AT1G08190) is observed at vacuole membranes only in the presence of the membrane lipid PI3P (Brillada *et al.* 2018). Together, these facts align with the linear scheme shown in Fig. 3A, where the process of fusion appears to emerge as a direct consequence of the presence of PI3P. The scheme implies that the absence of PI3P would prevent recruitment of HOPS subunits to the vacuole membrane and would thus prevent chaperoning of the *trans*-SNARE fusion complex. However, our experiments yielded the unexpected observation that PI3P depletion causes vacuoles to fuse. Given that linear reasoning about the molecular mechanisms underlying vacuole fusion failed to explain the reality of the biology, we sought an alternative mechanism that could capture the complex outcomes observed—and do so while remaining consistent with our prior knowledge about the molecular players in the system.

We began by asking what additional complexity might have been overlooked in our simple, linear description of the

biological mechanism. For one, if HOPS chaperones SNARE proteins into a *trans*-SNARE complex, then there is, at some point, a HOPS:*trans*-SNARE super-complex. This complex's existence was previously implicit in the chaperoning event (event 3 in Fig. 3A). Making it explicit in the model compels us to ask whether the HOPS:*trans*-SNARE super-complex is competent for facilitating fusion. The alternative would be to posit that the bare *trans*-SNARE complex is the fusion-competent assembly. We proceeded with this second assumption, which creates a requirement for HOPS to be removed from the super-complex. Following the principle of parsimony, we adopted the simplest possible explanation for HOPS removal—namely, spontaneous dissociation (Fig. 3B, event 4). If two species can spontaneously dissociate, it is reasonable to consider the possibility of reassociation (Fig. 3B, event 5). Finally, we made explicit the events that follow membrane fusion. After two membranes join, the SNARE complex has all members co-located in the same membrane, as a *cis*-SNARE complex. This must be disassembled to prime free SNAREs to participate in new vacuole-bridging complexes that drive subsequent rounds of vacuole fusion. We combined the events of fusion, disassembly and priming into a single abstracted event 6, as shown in Fig. 3B.

This non-linear scheme offers a potential explanation for the fusion response observed in the wortmannin experiment. If the fusion-competent species is the bare *trans*-SNARE complex, once the HOPS:*trans*-SNARE super-complex is formed, any perturbation that promotes the dissociated state will lead to fusion activity. If dissociation of the super-complex were reversible, an excess of HOPS in the membrane would tend to keep the *trans*-SNARE complex in the super-complex state. Conversely, any perturbation that reduces HOPS abundance in the membrane would promote the accumulation of the fusion-competent *trans*-SNARE machinery. In this schematic, two competing processes determine HOPS abundance in the membrane: HOPS subunit recruitment (event 1), which requires PI3P, and HOPS turnover from the membrane (event 2), which we assume to proceed at some basal rate. Depleting PI3P would put a stop to HOPS recruitment, leaving the turnover process to eliminate HOPS from the vacuole membrane. If turnover were sufficiently rapid, the result would be a swift release of fusion-competent *trans*-SNARE complexes and corresponding fusion activity.

While this conceptual model may explain the wortmannin experiment, it does not allow for fusion in the presence of PI3P. As PI3P depletion is a consequence of a lab-based chemical perturbation and is not known to be a feature of vacuole fusion in the native plant, the model is, at best, incomplete. However, the framework defines a hypothetical function required to complete the formation of fusion-competent SNARE complexes—one that enables a search for a missing signal in our biological mechanism.

2.3 Conceptual model suggests a missing signalling event, and yeast vacuole fusion offers a candidate signal

Our conceptual model suggests that HOPS removal could be a critical event to activate the *trans*-SNARE complex. Thus, we posited that the native stoma might possess an active mechanism for HOPS displacement from fusion complexes. While absent from the *Arabidopsis* literature, we found evidence of such stalling and activation phenomena amongst the comparatively well-studied proteins involved in yeast vacuole fusion. Specifically, we noted the example of Sec17 (SGD:S000000146), an alpha NSF attachment protein (α-SNAP) with a multifaceted role in yeast membrane fusion (Zick *et al.* 2015; Schwartz *et al.* 2017; Song *et al.* 2017; Jun and Wickner 2019; Song and Wickner 20192021). Sec17 facilitates rapid fusion when added to mixtures of stalled intermediate complexes in reconstituted proteoliposome experiments (Zick *et al.* 2015; Song *et al.* 2021) involving truncated SNARE proteins that cannot fully zipper together to drive membrane fusion. Interactions between membrane lipids and an apolar loop on Sec17 lower the energy barrier for membrane rearrangement, thereby encouraging fusion (Zick *et al.* 2015).

Given this information, we asked whether *Arabidopsis* possesses homologues of yeast Sec17. A BLASTP search of the *Arabidopsis* genome returns two loci with high similarity to Sec17: one locus with two isoforms (AT3G56190, *E* values of 3e-38 and 1e-29) and another with one form (AT3G56450, *E* value of 5e-15). These loci are annotated as ASNAP/ALPHA-SOLUBLE NSF ATTACHMENT PROTEIN (SNAP)2 (AT3G56190) and ALPHA-SNAP1 (AT3G56450). Roles for these proteins in the *Arabidopsis* fusion apparatus have not been reported, but a role in gametogenesis for ASNAP/ALPHA-SNAP2 has been established by Liu *et al.* (2021). Finally, both ASNAP1 and ASNAP2 transcripts are present in *Arabidopsis* guard cells (Pandey *et al.* 2010; Waese *et al.* 2017). Thus, we adopted Sec17 as a candidate signal for displacement of HOPS from HOPS:*trans*-SNARE super-complexes, as depicted in the updated model shown in Fig. 4. However, we wish to reiterate our hypothesis concerns a functional role, not a specific protein. While these proteins are strong candidates, it may be the case that another protein besides ASNAP1 or ASNAP2 performs this function in *Arabidopsis*. Notwithstanding, the schematic in Fig. 4 informs the remainder of this investigation.

Determining the validity of this conceptual model requires that we confront it with empirical data. To this end, we turned the diagram in Fig. 4 into a system of differential equations that we could simulate to predict emergent outcomes under different perturbations. The equations, reported in the detailed methods section, reflect the evolution of membrane protein abundances and configurations over time. When non-dimensionalized, the system of equations featured eight parameters. Table 1 defines those parameters, along with their associated events in the conceptual model.

The only data available to inform the model (Fig. 2) report on the evolution of vacuole morphology and do not capture the kinetics of individual events represented in the model. Parameter inference approaches can be used to reverse engineer parameter values based on known systems-level outcomes. However, that typically involves quantitative observations, and, preferably, time-series data of sufficient quality and quantity to render parameters practically identifiable. With only qualitative phenotypic observations to work with, we questioned whether that information could meaningfully constrain the parameterization of our proposed model and whether we could learn anything about the properties of the molecular signalling pathway from the available data.

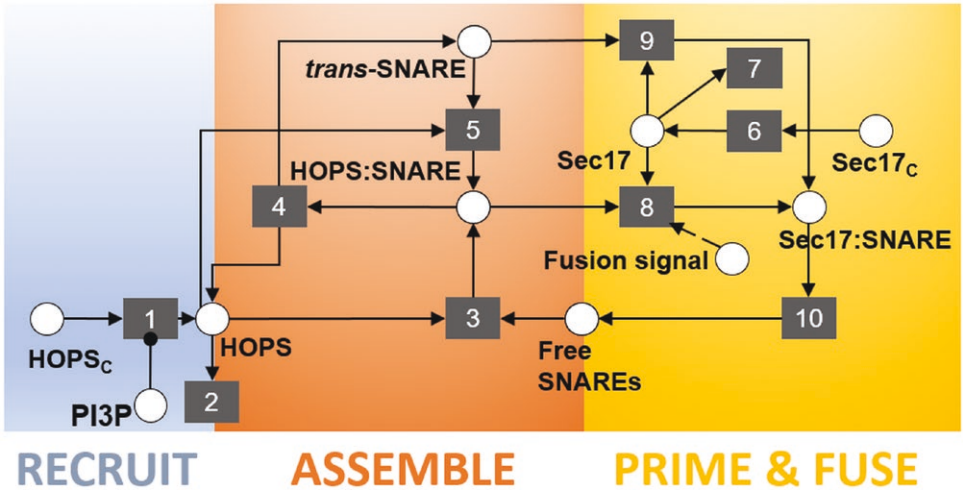

Figure 4. The final schematic offers the hypothesis that HOPS displacement is required to activate the *trans*-SNARE complex and drive fusion. The literature on yeast vacuole fusion offers a candidate signal with precisely that function—that is activating assembled, but inactive, trans-SNARE complexes. Furthermore, the *Arabidopsis* analogue of that yeast protein is expressed in guard cells. In our schematic, this protein, Sec17, is a cytoplasmic species recruited to the membrane (event 6), where it can associate with and activate *trans*-SNARE complexes (event 9). We posit that Sec17 cannot displace HOPS from HOPS:*trans*-SNARE super-complexes until the system receives some upstream signal that triggers stoma opening (event 8). After HOPS displacement, the fusion-competent complex drives fusion events (event 10). We allow the abstraction in event 10 to be inclusive of post-fusion phenomena such as the disassembly of the *cis*-SNARE complex, freeing individual SNARE proteins to participate in further rounds of fusion. Event 7 represents the turnover of Sec17 from the membrane. Events 1–5 are retained from earlier schematics (Fig. 3).

Table 1. Model parameters and their descriptions.

Parameter	Corresponding event	Description
K_1	1,2	Rates of HOPS recruitment and turnover
K_3	3	Chaperoning rate
K_4	4	Rate of HOPS:*trans*-SNARE super-complex dissociation
$a\ (=K_5/K_4)$	5	HOPS & *trans*-SNARE reassociation rate expressed relative to HOPS:*trans*-SNARE dissociation rate
K_6	6	Rate of Sec17 recruitment
K_7	7	Rate of Sec17 turnover
$\beta\ (=K_8/K_9)$	8	Rate for Sec17 displacement of HOPS expressed relative to rate for Sec17 association with *trans*-SNARE complexes
K_9	9	Rate of Sec17 association with *trans*-SNARE complexes

2.4 Vacuole morphology, as a qualitative phenotype, constrains model parameterization

As a first attempt to assess whether the existing observations might meaningfully constrain model parameterization, we ran simulations using parameter values randomly sampled across a large range spanning eight orders of magnitude. While sampling ~10^5 different parameter sets could not even begin to meaningfully explore the eight-dimensional parameter space, this cursory assessment did shed some light on whether the expected fusion characteristics are trivial to produce. To this end, we specified semi-quantitative emergent behaviours that the simulations would need to produce for the predictions to match our biological observations. We defined a match as any simulation that met five criteria: (1) the system must have a stable steady state prior to any perturbation causing fusion activity; (2) the system should exhibit increased fusion activity upon removal of PI3P; (3) the system should exhibit increased fusion activity upon triggering of event 8, our hypothetical mechanism of fusicoccin-responsive fusion; (4) fusion due to PI3P removal should occur more quickly than fusion due to trigger activation; (5) spontaneous fusion events in the absence of a specific signalling perturbation should be rare. We converted these qualitative statements into quantitative criteria (CR_i) by setting numerical thresholds (TH_i) for acceptance of any given simulation. Table 2 details these acceptance criteria, expressed as inequalities. We note the proportion of sampled parameter sets that satisfice each criterion. Here, we use the term satisfice to emphasize that our approach does not try to optimize a simulation outcome, but rather accepts as equally viable any parameterization that meets or surpasses our minimum—and quite conservative—requirements.

As our model can only report the instantaneous flux associated with the fusion event (i.e. a rate proportional to the abundance of [Sec17:SNARE], as indicated by event 10 in Fig. 4), we

Table 2. Translating qualitative phenotype observations into quantitative constraints.

Phenotypic constraint (CR*i*)		Mathematical interpretation	Percent of sampled parameter sets that satisfice criterion
CR_1	Prior to signal perturbation, the system should exhibit a stable steady state.	$d/dt_{\text{all species}} \leq 10^{-8}$	56.4
CR_2	PI3P depletion induces fusion.	$\frac{\int [Sec17{:}SNARE]_{\text{PI3P depletion}}\, dt}{\int [Sec17{:}SNARE]_{\text{no perturbation}}\, dt} \leq 0.1$	9.7
CR_3	Trigger activation induces fusion.	$\frac{\int [Sec17{:}SNARE]_{\text{trigger activation}}\, dt}{\int [Sec17{:}SNARE]_{\text{no perturbation}}\, dt} \leq 0.1$	24.0
CR_4	Fusion due to PI3P depletion should be faster than that due to trigger activation.	$\frac{\int [Sec17{:}SNARE]_{\text{trigger activation}}\, dt}{\int [Sec17{:}SNARE]_{\text{PI3P depletion}}\, dt} \leq 0.5$	20.2
CR_5	In the absence of an external signal, spontaneous fusion events should be rare.	$[Sec17:SNARE]\|_{\text{no perturbation}} \leq 10^{-6}$	6.9
All criteria satisficed concurrently			0.1

chose to quantify cumulative fusion activity as the integral under the curve of fusion rate versus time. For a given parameter set, we compared these integrals across simulations performed without a signal perturbation to those with a signal perturbation. As we had no quantitative data on relative fusion dynamics, we selected very conservative thresholds for the expected changes in fusion activity. For example, for criterion 2, when we simulated PI3P removal, we accepted any simulation increasing fusion activity by 10-fold or greater. Biological intuition suggests that a 10-fold increase is likely insufficient to explain our guard cell observations. If vacuole fusion takes place within 20 min (Fig. 2), and that process involves fusion activity only 10-fold greater than that in untreated cells, one might expect to see vacuoles fuse spontaneously in untreated cells over a several hours. This does not occur, so our chosen threshold is likely overly permissive. However, an overly restrictive threshold might elide regions of parameter space that are, in truth, biologically relevant. We chose to err on the side of permissiveness.

Table 2 reports the mathematical definitions of our criteria and our chosen acceptance thresholds. We accepted as plausible any parameterization that produced simulation results that met these thresholds. In this table, we also detail the fraction of the evaluated parameter sets that returned emergent dynamics matching this quantitative interpretation of our qualitative biological observations. These fractions were determined by evaluating model outcomes for $N = 2^{18}$ points in the eight-dimensional parameter space. We generated these samples using uniform Sobol' sampling (*sobolset* function in MATLAB) and found that less than 1% of the examined parameter sets produced simulation outcomes matching all five of our desired emergent behaviours. As fully satisficing parameter sets were scarce, we posited that our conservative criteria, expressed as inequalities, may be sufficient to constrain parameterization of our model. The parameters would clearly not be uniquely identifiable, but we should be able to discriminate sub-domains of parameter space that return biologically plausible kinetics. Interrogation of those sub-domains could then indicate experimentally tractable measurements that would permit us to establish the viability of our hypothesized signalling pathway. A simulation-based inference approach such as approximate Bayesian computation can enable a search for those domains by identifying plausible parameter values.

Other disciplines have developed conceptually similar strategies, such as the pattern-oriented modelling approaches used to interpret agent-based simulations of ecological behaviour (Wiegand *et al.* 2003; Grimm *et al.* 2005; Gallagher *et al.* 2021). More recently, a structural-functional plant model has been used to identify parameter values capable of reproducing quantitative emergent outcomes. This was achieved via forward simulation from 10^4 randomly sampled parameter sets (Wang *et al.* 2018, 2020). Our approach stands apart in that we solve the inverse problem—reverse-engineering credible parameter distributions within an N-dimensional parameter domain, and we do so by applying qualitative constraints to evaluate the parameter space of a deterministic dynamic model.

2.5 Simulation-based inference delineates plausible regions of parameter space

As we approached the problem of parameterizing this model, we first determined whether the model might be insensitive to any of the eight parameters. If so, one could fix the value of one or more parameters and thereby simplify our search for plausible kinetic constants. To this end, we performed a Sobol' global sensitivity analysis using the correlation-based approach of Glen and Isaacs (2012). This variance-based approach returns indices indicating how much each model parameter contributes to the variance of each simulation outcome. Performing the analysis required that we turn our simulation acceptance criteria into quantitative metrics indicating how far a given simulation is from satisficing the established criteria. We chose to translate each criterion and its acceptance threshold via a RelU objective function, as indicated in Equation (1). This formulation has the benefit of mapping all results meeting the acceptance threshold to identical scores of zero while penalizing results that do not meet our thresholds. Failing simulations will return scores that increase linearly as the simulation outcomes increasingly deviate from our desired behaviours. Using these functions as the outcomes evaluated in the Sobol' analysis allowed us to evaluate how each model parameter contributed to a decision as to whether a simulation would produce satisficing emergent behaviours.

$$O_i = RelU\left(\frac{CR_i - TH_i}{TH_i}\right). \quad [1]$$

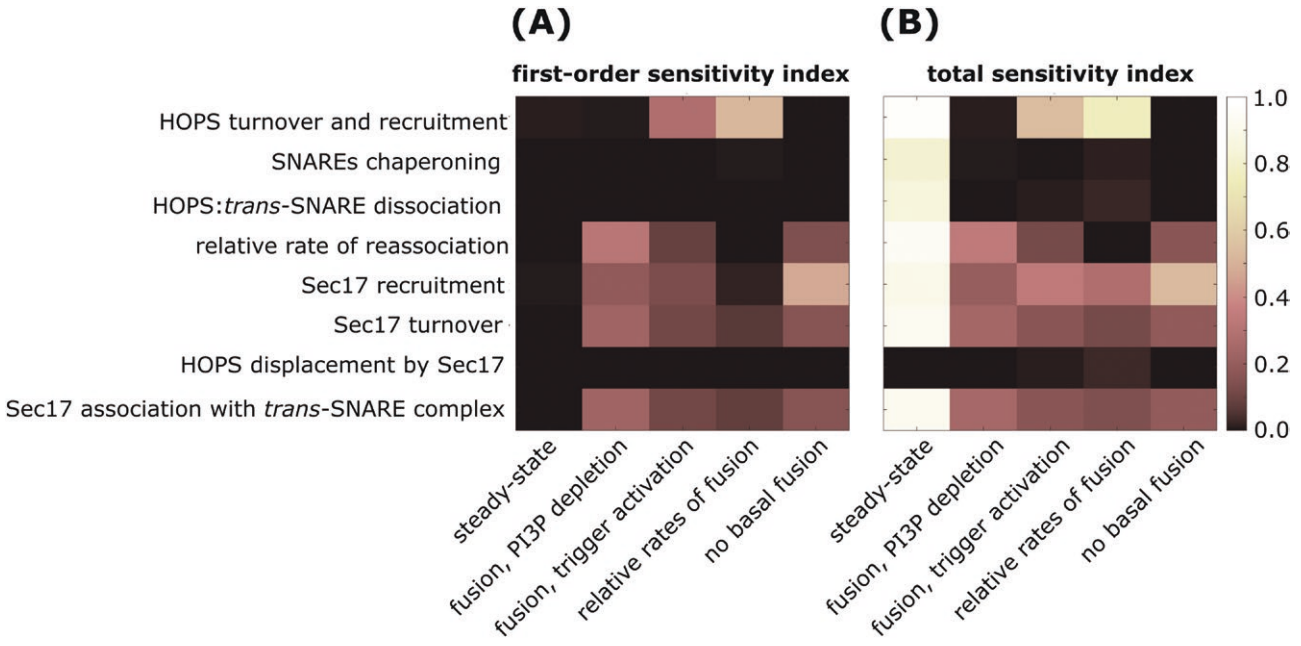

Figure 5. Variance-based global sensitivity analysis. (A) First-order indices, indicating what fraction each model parameter (*y* labels) independently contributes to the variance of each model outcome (*x* labels). (B) Total Sobol' indices indicate each parameter's contribution to the variance of each outcome when considering all inter-parameter interactions. We calculated the Sobol' indices using two independent sets of $N = 10^5$ samples. Results indicate that all parameters make a statistically significant contribution to satisficing the desired model outcomes. However, the contribution of the rate constant for HOPS displacement by Sec17 is weak across all outcomes, and the SNARE chaperoning rate has little impact on fusion dynamics. Seven of the eight parameters strongly impact the steady-state criterion, but they do so almost exclusively through parameter interactions.

Fig. 5 reports our estimates of the first order and total sensitivity indices. We note that acceptance of the steady state criterion appears insensitive to all parameters when only first-order effects are considered. However, when second- and higher-order parameter interactions are included (i.e. in the total sensitivity index), the steady-state requirement exhibits the greatest sensitivity to all parameters. Although the parameter describing the rate constant for Sec17 displacement of HOPS contributes little variance to satisfaction of our five outcomes of interest, the parameter's impacts on outcomes 3 and 4 (relative rates of fusion under different treatments and expectations for basal fusion, respectively) are significantly different from zero, as determined by a Wilcoxon Rank Sum test ($T_i = 0.009$ and 0.03, respectively; $P <$ 1e-6. Approach detailed in "Methods" section). Note that these values do not reflect absolute sensitivity, but rather indicate each parameter's relative contribution to the overall variance of each model outcome. Given the results of this sensitivity analysis, we chose to estimate all eight parameters.

Using our objective functions as indicators of valid emergent dynamics, we attempted to infer plausible regions of parameter space for our model. To achieve this, we used the Bayesian inference approach described by Toni *et al.* (2009) —namely, Approximate Bayesian Computation using Sequential Monte Carlo (ABC-SMC). This algorithm requires a distance metric to quantify the deviation of a simulation outcome from a target value. Given our desire to satisfice multiple outcomes simultaneously, we summed the five objective functions, defined as per Equation (1), to give a single summary statistic. With this definition, the target value for our summary statistic was zero. We used a uniform perturbation kernel, $N = 5000$ particles, and a schedule that reduced the rejection constant by 10% for each successive particle population. Further details on our implementation of the ABC-SMC algorithm can be found in the Methods section.

To assess the reproducibility of our parameter inference strategy, we performed two independent ABC trials that differed in their randomly generated initial particle population. We tested reproducibility by performing two-sample Kolmogorov–Smirnov hypothesis tests on the paired marginal distributions obtained in the two trials ($\alpha = 0.05$). The two trials exhibited no statistically significant difference in the distributions inferred for any parameter (P values ranged from $[0.218, 0.758]$). Thus, we concluded that the results were representative and reproducible. Fig. 6 depicts the inferred marginal distributions for each model parameter, and Table 3 reports the corresponding 95% credible intervals (CI).

Although no parameters were well-constrained, our inference approach did identify plausible sub-domains in parameter space. Alternatively, one could say that we effectively excluded implausible domains that would not be worthy of further interrogation. Having searched over eight orders of magnitude, our ABC-SMC algorithm found plausible values ranging over 2–7 orders of magnitude (Table 3). On the more-constrained end of the scale, α (the relative rate of HOPS and SNARE reassociation) and β (the relative rate of HOPS displacement by Sec17) varied over 2–3 orders of magnitude. At the other extreme, inferred values for K_4 (the HOPS:*trans*-SNARE dissociation rate), K_6 (the Sec17 recruitment rate), K_7 (rate of Sec17 turnover from the membrane) and K_9 (the rate of Sec17 association with bare

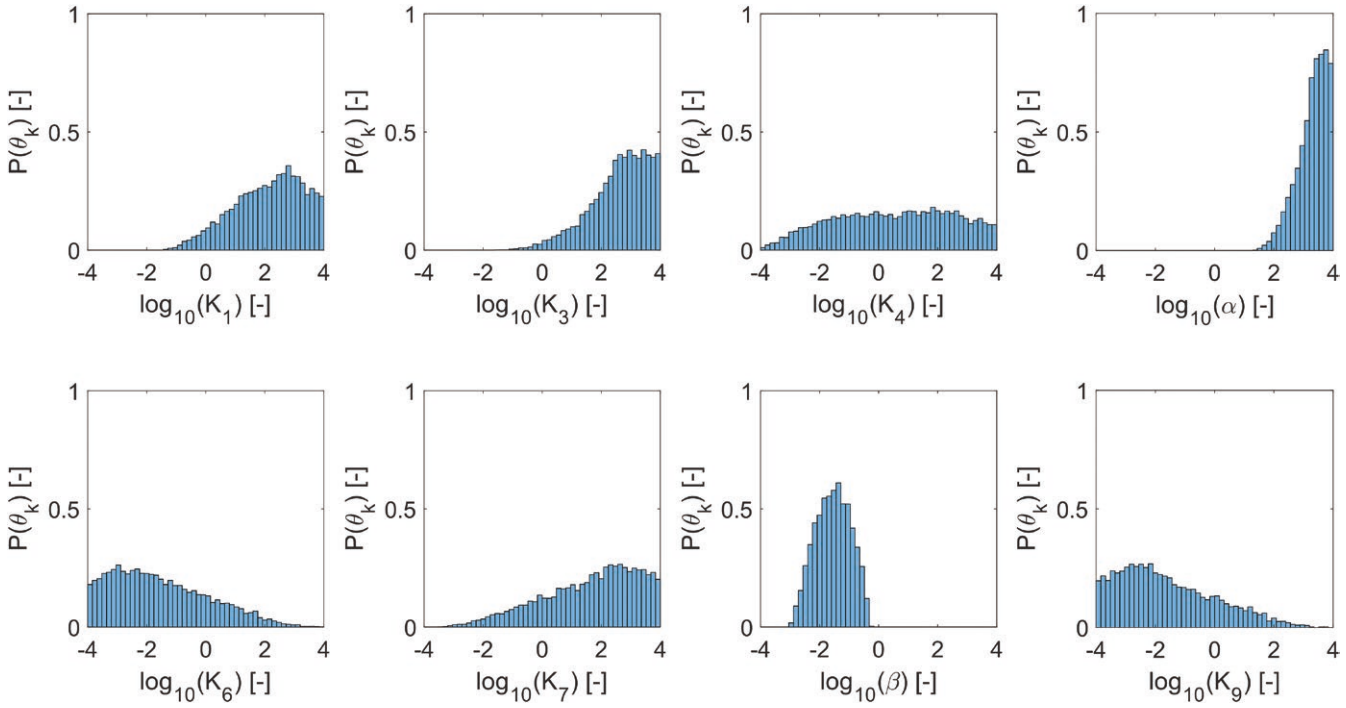

Figure 6. Marginal distributions indicate plausible parameter values, as inferred via approximate Bayesian computation. Inference was performed for two independent replicates using a particle population of 5000 parameter sets each. Plausible parameter sets are those that allow the model to satisfice all five criteria presented in Table 2 (see Table 1 for parameter descriptions). Satisficing these criteria implies that the model recapitulates the experimental observations of interest. The plots represent the final particle populations from both replicates, yielding histograms reflecting $N = 10\,000$ satisficing parameter sets.

Table 3. Ninety-five percent CIs for plausible parameter values, as inferred via approximate Bayesian computation. Values are reported as $\log_{10}(\theta)$.

Parameter	95% credible interval
K_1	[-0.38, 3.9]
K_3	[0.25, 3.9]
K_4	[-3.2, 3.8]
α (=K_5/K_4)	[2.1, 4.0]
K_6	[-3.9, 2.0]
K_7	[-1.9, 3.9]
β (=K_8/K_9)	[-2.7, -0.51]
K_9	[-3.9, 1.9]

trans-SNARE complexes) extended across at least six orders of magnitude. Indeed, the marginal distribution for K_4 exhibited plausible values across nearly the full range examined. Despite the broad range of values deemed plausible, we learned general emergent principles when we examined the relationships between parameter pairs by plotting 2D histograms.

The kinetic quantities reported in Table 3 may tempt one to map our non-dimensional parameter domains to biologically meaningful values. However, the degree of uncertainty inherent in these parameter estimates makes it inappropriate to seek meaning from the specific kinetic values. We instead achieve sensemaking only from relative kinetics and emergent properties that are robust across the parameter sets identified.

2.6 Model predicts that closed stoma exhibits stalled trans-SNARE fusion complexes

As indicated by the inferred values for α, our ABC-SMC process identified plausible parameter domains where HOPS and SNARE complexes reassociate with a rate constant greater than the HOPS:*trans*-SNARE super-complex dissociates. While we found plausible values for the HOPS:*trans*-SNARE dissociation rate, K_4, throughout the interrogated parameter range, we consistently observed that the reassociation rate was 2–4 orders of magnitude faster (Table 3). Indeed, an associated finding was the predominance of protein super-complexes rather than HOPS absence or free SNARE proteins in the pre-fusion steady state. A survey of the model's steady state across all 10 000 inferred parameter sets consistently returned the result that HOPS complexes are in HOPS:*trans*-SNARE super-complexes prior to fusion signalling (95% CI for free HOPS abundance relative to HOPS:*trans*-SNARE super-complexes: [0.952, 0.952]). Our simulations similarly predicted that SNARE proteins are almost exclusively in super-complexes rather than the free SNARE state (95% CI: [0.992, 1.00]). From this, we offer the testable hypothesis that HOPS should be observed in the vacuole membranes of closed stoma. Furthermore, an appropriate biophysical experiment—such as FRET-FLIM, bimolecular fluorescence complementation (BiFC), or co-immunoprecipitation (Co-IP)—should provide evidence of membrane HOPS being associated with SNARE proteins. Again, this would be in the closed stoma, and, if observed, would indicate that HOPS recruitment and chaperoning of the SNARE complex do not require a stoma opening signal.

The other key protein in our simulations is Sec17. We observed that the predicted abundance of Sec17 in the membrane is consistently lower than that of HOPS. Upon surveying the ratio of total membrane Sec17 to total HOPS across simulations based on our inferred parameter sets, we obtained steady-state values of 5.0e-5 (median; 95% CI: [2.2e-8, 0.017]). Inspecting the plausible parameter sets indicates this may be due to differences in protein recruitment rates. When we examined the 2D histogram of HOPS and Sec17 turnover rates (K_1 and K_7, respectively), we found that turnover rates for the proteins may be comparable (Fig. 7A). If not comparable, either protein might exhibit the greater rate of turnover. However, the relationship between rates of recruitment was less ambiguous. Two-D histograms suggest that HOPS and Sec17 recruitment rates (K_1 and K_6, respectively) may differ considerably (Fig. 7B). Indeed, the modal outcome corresponds to HOPS being recruited at rates ~5 orders of magnitude faster than Sec17. With Fig. 7C, we introduce the additional observation that Sec17 turnover is typically faster than Sec17 recruitment (Fig. 7C). From these observations, we offer the testable hypothesis that Sec17 should not be readily observed in the vacuole membranes of closed stoma. However, not seeing the protein under these conditions should not be misconstrued as implying that Sec17 could not have a role in vacuole membrane fusion.

Finally, our model frames the guard cell treatments that induce fusion as doing so via two different paths: one that proceeds by Sec17 engaging spontaneously with *trans*-SNARE complexes, and one that proceeds via Sec17 actively displacing HOPS from the HOPS:*trans*-SNARE super-complex (via events 8 and 9, respectively, in Fig. 4). Via our inference algorithm, we estimated β—the ratio between the rate constants governing these paths (K_8/K_9). We observed this value to be consistently negative in log space (median -1.5; 95% CI [-2.7, -0.51]). The inferred range of values implies that the process requiring HOPS displacement proceeds at less than half the rate that it would if the *trans*-SNARE complex were not associated with HOPS (median ratio of 0.029; 95% CI: [0.0022, 0.31]). This suggests that Sec17 association with *trans*-SNARE complexes is hindered by the presence of HOPS.

2.7 Modelling positions HOPS as a dual regulator of guard cell vacuole fusion, encouraging formation of the trans-SNARE fusion complex, but stalling the complex's activity

By carefully integrating our knowledge of the molecular machinery involved in vacuole fusion with our observations of emergent vacuole morphology, we have arrived at a novel hypothesis (Fig. 8) regarding the function of HOPS in plant guard cells. We predict that HOPS complexes promote the formation of a stable HOPS:*trans*-SNARE super-complex, but that super-complex

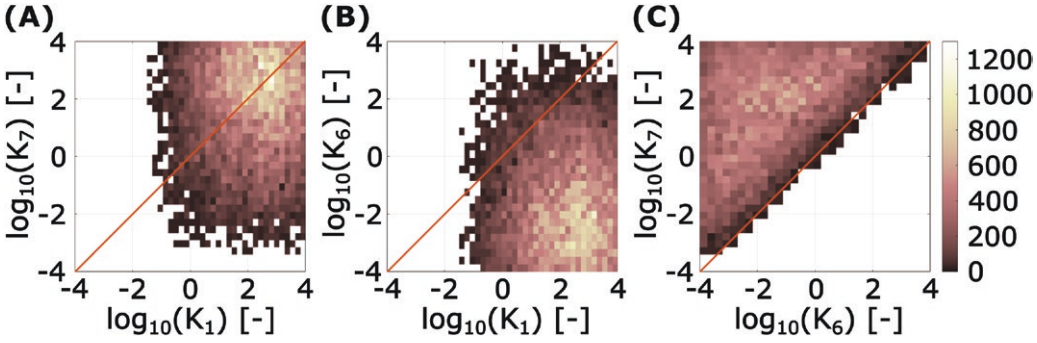

Figure 7. Plausible parameter domains indicate distinguishing recruitment rates for membrane HOPS and Sec17. Two-dimensional histograms depicting parameter values that satisfice all simulation criteria. (A) HOPS and Sec17 turnover rate constants (K_1 and K_7, respectively). (B) HOPS and Sec17 recruitment rate constants (K_1 and K_6, respectively). (C) Rate constants for Sec17 recruitment and turnover (K_6 and K_7, respectively). Plots represent combined parameter sets from two ABC trials, giving a total of $N = 10^4$ parameter sets satisficing all simulation criteria (see Table 2).

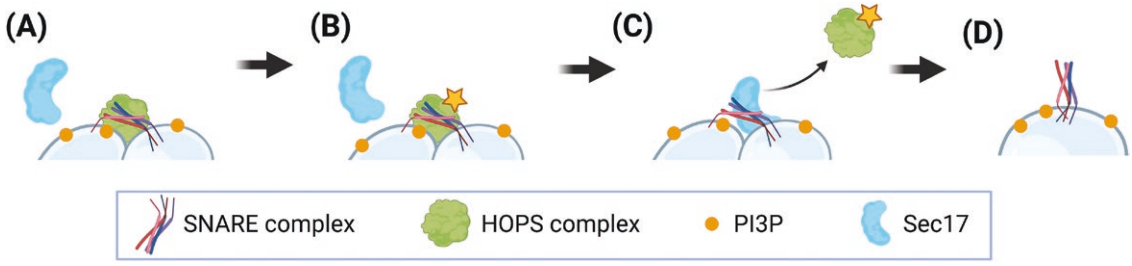

Figure 8. Modelling positions HOPS as a dual regulator of guard cell vacuole fusion. (A) The presence of PI3P permits HOPS recruitment to the membrane. There, HOPS promotes the formation of the *trans*-SNARE fusion machinery but then prevents fusion activity by hindering the access of Sec17. (B) A biological signal capable of reducing HOPS:*trans*-SNARE binding affinity (e.g. a signal resulting in the post-translational modification of a HOPS subunit, as indicated by the star icon) could create the conditions required for Sec17 to displace HOPS and (C) thereby activate the otherwise stalled fusion complex, resulting in (D) membrane rearrangement and vacuole fusion.

cannot facilitate fusion until an appropriate signal is perceived. We thus frame a regulatory role for HOPS that is distinct from its chaperoning activity. Chaperoning helps form the fusion machinery, but our model suggests that this event is decoupled from fusion activity. In fact, analysis of the model indicates that the presence of HOPS hinders fusion activity. Furthermore, a sensitivity analysis constrained to the model's plausible parameter domains indicates that the fusion rate may be insensitive to the chaperoning rate. We thus posit that a biological signal capable of triggering fusion should ultimately impact the HOPS:*trans*-SNARE super-complex, and it should do so by facilitating HOPS displacement. This impact could arise via changes in HOPS/SNARE binding affinity or Sec17/SNARE interactions. Such a change could, in turn, be induced by post-translational modification of a relevant protein—for example, a HOPS subunit. Whether this change is mediated by phosphorylation status, an allosteric regulatory interaction, or another mechanism as yet unknown remains a topic for future investigation.

Finally, we note that the proposed scheme positions the signal for vacuole fusion as one acting downstream of forming the *trans*-SNARE fusion complex. For example, in the plant-specific phenomenon of stomatal response to daylight, this mechanism would allow the plant to pre-dock pairs of fragmented vacuoles by forming stalled *trans*-SNARE complexes overnight. The system would then be poised to respond rapidly at daylight by producing a burst of fusion activity to support guard cell swelling and stomatal opening.

2.8 Conclusion

We began this study with the unexpected biological observation that chemical depletion of a specific phosphoinositide—one apparently required to assemble fusion machinery in guard cells—induces fusion. Using simulation-based inference, we integrated existing biological knowledge with scarce phenotypic data to establish plausible kinetics associated with a candidate systems model. As data to inform the model, we considered the observed state of vacuole fragmentation in live cells under two lab-based perturbations: (i) a fusicoccin treatment that mimics the normal cues for stoma opening and (ii) a wortmannin treatment that depletes the regulatory lipid of interest, PI3P. Taking this phenotypic data to be evidence of relative fusion rates, we implemented a model that predicts fusion activity emerging from a multi-step signalling pathway. Our observations regarding the state of fragmentation were few and qualitative, but they proved sufficient information to constrain a search for plausible model parameters.

Using an ODE model to make forward predictions and a Bayesian inference approach to reverse engineer governing parameters, we characterized those regions in the model's multidimensional parameter space that are consistent with the expected fusion dynamics. Then, by sampling from that domain of plausible kinetics, we generated falsifiable mechanistic hypotheses regarding the intracellular localization of HOPS and SNARE complexes prior to fusion. We predicted that the apparently contradictory observation that PI3P is required for fusion, but removing PI3P promotes spontaneous fusion in plants, can be resolved by positing that HOPS and SNARE proteins exist as pre-formed, but stalled, HOPS:*trans*-SNARE super-complexes in the guard cells of closed stoma. Our work thus positions HOPS as having a dual role in regulating *trans*-SNARE fusion complexes in *Arabidopsis* guard cells. Namely, HOPS acts as both a promoter and inhibitor of vacuole fusion, executing these roles at different points in the non-linear signalling pathway that regulates vacuole fusion. We propose that the HOPS complex chaperones individual SNARE proteins into their *trans*-SNARE fusion machinery and then acts as a brake on the function of that machinery. Environmental cues for stoma opening would then act as a signal to release that brake.

Our model also introduces a functional role for a protein acting to displace HOPS from the *trans*-SNARE complex. This protein interacts with *trans*-SNARE assemblies to form a fusion-competent complex capable of rearranging membranes. By leveraging information from other kingdoms of life, we inferred that the yeast protein Sec17 could serve this function. Furthermore, apparent homologues of Sec17 (ASNAP1 and ASNAP2) exist in *Arabidopsis*. In addition, ASNAP2 has been shown to interact with the vacuolar Qa SNARE SYP22 in root tissue isolates (Fujiwara *et al.* 2014). We suggest that research efforts focussed on the proteins ASNAP1 and ASNAP2 would be useful avenues for future investigation using protein–protein interaction assays. For now, whether ASNAP proteins interact with the specific SNARE hetero-tetramer involved in guard cell vacuole fusion remains unknown.

In addition to the insights documented here, our proposed model for vacuole fusion dynamics lays the foundation for future research as a tool for hypothesis generation. This will facilitate the study of protein functions and interactions that would otherwise be difficult to track experimentally. Finally, future validation of this model may eventually lead to genetic applications to increase water use efficiency in dicot crop systems.

3. METHODS

3.1 Plant growth conditions and stomata assays

Wild-type *Arabidopsis thaliana* ecotype Columbia-0 (Col-0) plants were grown in soil at 22 °C with a 16 h photoperiod. Leaves from 4-week-old plants were cut in the morning and immediately processed to generate epidermal peels as described (Schroeder *et al.* 1993; Behera and Kudla 2013; Li *et al.* 2013) with modifications. Briefly, a small leaf fragment was applied abaxially to a coverslip coated with medical adhesive, and all but the bottommost layers of abaxial cells containing the stomata were scrapped away with a razor. One millimetre thick silicone isolators (GraceBio #664170) were used to create wells around the adhesive for incubations. Epidermal peels were immediately incubated in stomata buffer (MES pH 6.1). To induce stomatal closure, peels were incubated in closing buffer (10 mM MES pH 6.1, 40 mM malate, 5 mM $CaCl_2$, 10 μM 2',7'-Bis-(2-CarboxyEthyl)-5-(and-6)-CarboxyFluorescein, Acetoxymethyl Ester (BCECF, Fisher Scientific B1170), 50 mM ABA (Sigma Aldrich A1049) at 22 °C in the dark for 2 h. To induce stomatal opening or vacuole fusion, ABA-treated peels were incubated in opening buffer (10 mM MES pH 6.1, 50 mM KCl) supplemented with 10 μM BCECF and either 3 μM fusicoccin (Sigma F0537) or 33 μM wortmannin (Sigma W3144). Wortmannin-treated peels were kept in the dark, whereas fusicoccin-treated peels were exposed to the light for up to 1 h. All concentrated stocks were first dissolved in DMSO. Images of leaf epidermal

Table 4. Dimensionless parameters and their definitions.

Event	Dimensionless rate constant	Definition
1	K_2	k_2/k_{10}
2	K_2	k_2/k_{10}
3	K_3	$k_3k_1^4/(k_{10}k_2^4)$
4	K_4	k_4/k_{10}
5	K_5	k_1k_5/k_2k_{10}
6	K_6	k_6/k_{10}
7	K_7	k_7/k_{10}
8	K_8	k_1k_8/k_2k_{10}
9	K_9	k_1k_9/k_2k_{10}
10	K_{10}	1

peels were acquired after ABA incubation and after 20, 40 and 60 min of fusicoccin or wortmannin treatments.

3.2 Microscopy

Confocal laser scanning microscopy was carried out in a Zeiss LSM 980 confocal microscope. Images were taken with a 40× FCS water objective (1.1 N.A.). Acquisition of BCECF fluorescence was accomplished with 405 nm laser excitation and 495–550 nm emission filter set. Images were acquired with an Airyscan detector with a pinhole size of 2.5 airy units.

3.3 Protein sequence comparisons

Sequence comparisons were performed using BLASTP 2.9.0+ comparing the Araport 11 protein dataset and the yeast protein sequence for Sec17 taken from the *Saccharomyces* Genome Database (SGD) (Schäffer *et al.* 2001; Cherry *et al.* 2012; Engel *et al.* 2014; Berardini *et al.* 2015; Cheng *et al.* 2017).

3.4 Governing equations of the mathematical model

Our model of consists of the following set of ODEs:

$$\frac{d\,[\mathrm{HOPS}]}{dt} = k_1\,\{\mathrm{HOPSc}\}\,\{\mathrm{PI3P}\} + k_4\,[\mathrm{HOPS:SNARE}] - k_5\,[\mathrm{HOPS}]\,[\mathit{trans}\mathrm{SNARE}] - k_3\,[\mathrm{HOPS}]\,[\mathrm{SNAREs}]^4 - k_2\,[\mathrm{HOPS}]$$

$$\frac{d\,[\mathit{trans}\mathrm{SNARE}]}{dt} = k_4\,[\mathrm{HOPS:SNARE}] - k_5\,[\mathrm{HOPS}]\,[\mathit{trans}\mathrm{SNARE}] - k_9\,[\mathrm{SEC17}]\,[\mathit{trans}\mathrm{SNARE}]$$

$$\frac{d\,[\mathrm{SNAREs}]}{dt} = 4 \times k_{10}\,[\mathrm{SEC17:SNARE}] - 4 \times k_3\,[\mathrm{HOPS}]\,[\mathrm{SNAREs}]^4$$

$$\frac{d\,[\mathrm{SEC17:SNARE}]}{dt} = k_9\,[\mathrm{SEC17}]\,[\mathit{trans}\mathrm{SNARE}] + k_8\,[\mathrm{SEC17}]\,[\mathrm{HOPS:SNARE}]\,\{\mathrm{biological\ signal}\} - k_{10}\,[\mathrm{SEC17:SNARE}]$$

$$\frac{d\,[\mathrm{HOPS:SNARE}]}{dt} = k_3\,[\mathrm{HOPS}]\,[\mathrm{SNAREs}]^4 + k_5\,[\mathrm{HOPS}]\,[\mathit{trans}\mathrm{SNARE}] - k_4\,[\mathrm{HOPS:SNARE}] - k_8\,[\mathrm{SEC17}]\,[\mathrm{HOPS:SNARE}]\,\{\mathrm{biological\ signal}\}$$

$$\frac{d\,[\mathrm{SEC17}]}{dt} = k_6\,[\mathrm{SEC17c}] - k_7\,[\mathrm{Sec17}] - k_8\,[\mathrm{SEC17}]\,[\mathrm{HOPS:SNARE}]\,\{\mathrm{biological\ signal}\} - k_9\,[\mathrm{SEC17}]\,[\mathit{trans}\mathrm{SNARE}]$$

The quantities enclosed in curly brackets are Boolean variables indicating whether the indicated species is present or absent. We abstracted the availability of cytosolic HOPS subunits into a single cytosolic species that we denote as HOPSc. We assume that VPS41 recruitment acts as the rate-limiting step for recruitment of all HOPS subunits to form the HOPS complex at the membrane. VPS41 is the subunit whose recruitment has been observed to be regulated by PI3P. Treating the HOPS subunits as abundant in the cytosol (i.e. with concentration not meaningfully altered by membrane recruitment) allowed us to fold the cytosolic abundance of HOPS into the rate constant for HOPS recruitment. We then treated the presence of cytosolic HOPS as a binary variable {HOPSc}.

We non-dimensionalized the system of ODEs using a concentration scale of k_1/k_2 (i.e. the ratio of the rate constants for HOPS recruitment from the cytoplasm and HOPS turnover from the membrane) and a time scale of $1/k_{10}$ (i.e. the inverse of the rate constant for fusion). The dimensionless rate constants and their constituent parameters are listed in Table 4. This scaling reduced the number of model parameters from nine to eight. It also allowed us to express all rate constants relative to that for the fusion event, which has a non-dimensional value of one. In our analyses, for all parameters in our dimensionless system of equations, we considered rate constants four orders of magnitude larger and four orders of magnitude smaller than this reference value of one.

3.5 Sobol' global sensitivity analysis

The Sobol' algorithm provides a point estimate of the Sobol' index associated with each parameter and outcome. However, efficient calculation of the Sobol' indices requires a numerical approximation involving many samples across the interrogated parameter domain. To determine whether each estimated index could credibly be differentiated from zero (at the chosen level of sampling), we introduced a dummy parameter and a dummy outcome to the analysis and used them as a control for true insensitivity. The dummy parameter does not feature in the systems model and thus provides a negative control for the sensitivity of model outcomes. We set the dummy outcome equal to one of the model kinetic parameters so that the dummy outcome provides an example of (i) perfect variance ($T_j = 1$) for that outcome-parameter combination and (ii) true insensitivity for all other parameters. We then used a Wilcoxon ranked sum test to determine whether, at a given sampling level, we could reject the null hypothesis that the distribution of bootstrapped sensitivity values for any given outcome-parameter pair has a median matching the negative control. We interpreted the rejection of

the null hypothesis (at a confidence level of $P < 0.05$) as evidence of a statistically significant sensitivity index.

3.6 Parameter estimation using ABC-SMC

We performed parameter estimation using approximate Bayesian computation with the sequential Monte Carlo (ABC-SMC) approach described by Toni *et al.* (2009). We began with an uninformative uniform prior (defined in log space) for every model parameter and used uniform Sobol' sampling to generate an initial population of $N = 5000$ particles. We then solved the system of ODEs and evaluated the summary statistic for each particle. As per the ABC-SMC algorithm, we randomly selected a particle for perturbation—initially using uniform weighting. The particle's parameters were then perturbed using a Markov kernel. We chose a uniform proposal kernel, $K(\theta_j^t \mid \theta_j^{t-1})$, defined as per Equation (2), where θ_j denotes the value of parameter j, t-1 denotes the current particle population and t denotes the subsequent population. This limited the perturbation range for parameter j to within a distance D of the parameter's current value. We defined D as $0.25\Delta_j$, where Δ_j is the range of θ_j values represented in the current particle population.

$$K(\theta_j^t \mid \theta_j^{t-1}) = U(\theta_j - D, \theta_j + D). \quad [2]$$

We rejected the proposed particle perturbation if the summary statistic evaluated for the perturbed parameter values exceeded a rejection constant, ε. Initially, we set the rejection constant to the 99th percentile of the summary statistics characterizing the particle population. We then reduced ε by 10% for each subsequent population (i.e. $\varepsilon_t = 0.9\varepsilon_{t-1}$). If the perturbed particle was rejected, we returned to the particle sampling step and repeated the process of particle selection, perturbation and evaluation until an acceptable perturbation was identified. We then assigned that accepted particle to the next particle population and iterated until we identified a complete set of N new particles. Subsequent rounds of particle perturbation employed importance sampling to weight the selection of candidate particles to perturb. By iteratively reducing the rejection constant, the algorithm moved each subsequent population closer to the target distribution we sought—that is, one that reflects a domain in parameter space plausibly describing our biological system. We iteratively generated new populations until 99% of the particles reflected a summary statistic of zero, where zero indicates a simulation that satisfies all acceptance criteria.

3.7 Programming languages and code availability

The codes for this model and associated analyses were written in MATLAB (R2022B) (The MathWorks, Inc., Natick, Massachusets, USA). Data and code used to generate the figures and perform the analyses for this paper are hosted at https://gitlab.com/hodgenscode/hodgens2023. A copy of the microscopy data has been made available at Zenodo at: https://zenodo.org/doi/10.5281/zenodo.10998767.

SUPPORTING INFORMATION

The following additional information is available in the online version of this article –

Supplemental Table 1. Guard cell vacuole fragmentation status. Images of BCECF-stained guard cell vacuoles were qualitatively assessed to determine their fragmentation status. Individual guard cells were annotated as either fragmented ("F"), unfragmented ("U"), intermediate ("M"), or un-callable ("N"). Each row provides the number of guard cells for a given combination of treatment condition, acquisition date, treatment time, peel number, and fragmentation status. Source images used for this analysis are available on Zenodo at: https://zenodo.org/doi/10.5281/zenodo.10998767.

ACKNOWLEDGEMENTS

We thank Xiaohan Yang for help reviewing this manuscript. Figs 1 and 8 were created using BioRender.com.

CONTRIBUTIONS BY THE AUTHORS

Investigation: C.H., B.S.A., M.R.P., D.T.F., I.K., A.M.P., L.M.G., N.J.E.; Conceptualization: B.S.A., M.R.P.; Funding Acquisition: B.S.A., M.R.P.; Writing-original draft: C.H., B.S.A.; Writing-review & editing: B.S.A., C.H., D.T.F., A.M.P., and M.R.P.; Methodology: C.H., B.S.A., D.T.F.; Software: C.H., D.T.F.;Formal Analysis: C.H., D.T.F.

CONFLICT OF INTEREST STATEMENT

None declared.

DISCLAIMER

This manuscript has been authored by UT-Batelle, LLC, under contract DE-AC05-00OR22725 with the US Department of Energy (DOE). The US government retains and the publisher, by accepting the article for publication, acknowledges that the US government retains a nonexclusive, paid-up, irrevocable worldwide license to publish or reproduce the published form of this manuscript or allow others to do so, for US government purposes. DOE will provide public access to these results of federally sponsored research in accordance with the DOE Public Access Plan (http://energy.gov/downloads/does-public-access-plan).

DATA AVAILABILITY

Code used to perform the analyses for this paper is hosted at https://gitlab.com/hodgenscode/hodgens2023. Microscopy data used to generate the figures has been made available at Zenodo at: https://zenodo.org/doi/10.5281/zenodo.10998767. Analyses were performed using MATLAB (R2022B).

FUNDING

This work was supported by the National Science Foundation (MCB-1918746 award to M.R.P. and B.S.A.). Co-author D.T.F. acknowledges fellowship support from NIH 5T32GM133366 (PIs Robert M. Kelly and Jason Haugh)..

LITERATURE CITED

Albert R, Acharya BR, Jeon BW, Zañudo JGT, Zhu M, Osman K, Assmann SM. 2017. A new discrete dynamic model of ABA-induced stomatal closure predicts key feedback loops. *PLoS Biology* 15:e2003451. doi:10.1371/journal.pbio.2003451.

Assmann SM, Schwartz A. 1992. Synergistic effect of light and fusicoccin on stomatal opening. *Plant Physiology* 98:1349–1355. doi:10.1104/pp.98.4.1349.

Behera S, Kudla J. 2013. Live cell imaging of cytoplasmic Ca2+ dynamics in *Arabidopsis* guard cells. *Cold Spring Harbor Protocols* 2013:665–669. doi:10.1101/pdb.prot072983.

Berardini TZ, Reiser L, Li D, Mezheritsky Y, Muller R, Strait E, Huala E. 2015. The Arabidopsis Information Resource: making and mining the 'Gold Standard' annotated reference plant genome. *Genesis* 53:474–485. doi:10.1002/dvg.22877.

Boeddinghaus C, Merz AJ, Laage R, Ungermann C. 2002. A cycle of Vam7p release from and PtdIns 3-P-dependent rebinding to the yeast vacuole is required for homotypic vacuole fusion. *Journal of Cell Biology* 157:79–90. doi:10.1083/jcb.200112098.

Bright NA, Lindsay MR, Stewart A, Luzio JP. 2008. The relationship between lumenal and limiting membranes in swollen late endocytic compartments formed after worthmannin treatment or sucrose accumulation. *Traffic* 2:631–642. doi:10.1034/j.1600-0854.2001.20906.x.

Brillada C, Zheng J, Krüger F, Rovira-Diaz E, Askani JC, Schumacher K, Rojas-Pierce M. 2018. Phosphoinositides control the localization of HOPS subunit VPS41, which together with VPS33 mediates vacuole fusion in plants. *Proceedings of the National Academy of Sciences of the United States of America* 115:E8305–E8314. doi:10.1073/pnas.1807763115.

Cao W, Li Z, Huang S, Shi Y, Zhu Y, Lai MN, Lok PL, Wang X, Cui Y, Jiang L. 2022. Correlation of vacuole morphology with stomatal lineage development by whole-cell electron tomography. *Plant Physiology* 188:2085–2100. doi:10.1093/plphys/kiac028.

Carballo-Pacheco M, Nicholson MD, Lilja EE, Allen RJ, Waclaw B. 2020. Phenotypic delay in the evolution of bacterial antibiotic resistance: mechanistic models and their implications. *PLoS Computational Biology* 16:e1007930. doi:10.1371/journal.pcbi.1007930.

Carter R, Woolfenden H, Baillie A, Amsbury S, Carroll S, Healicon E, Sovatzoglou S, Braybrook S, Gray JE, Hobbs J, Morris RJ, Fleming AJ. 2017. Stomatal opening involves polar, not radial, stiffening of guard cells. *Current Biology* 27:2974–2983.e2. doi:10.1016/j.cub.2017.08.006.

Chen YA, Scheller RH. 2001. SNARE-mediated membrane fusion. *Nature Reviews Molecular Cell Biology* 2:98–106. doi:10.1038/35052017

Cheng C, Kirkpatrick M. 2019. Inversions are bigger on the X chromosome. *Molecular Ecology* 28:1238–1245. doi:10.1111/mec.14819.

Cheng CY, Krishnakumar V, Chan AP, Thibaud-Nissen F, Schobel S, Town CD. 2017. Araport11: a complete reannotation of the *Arabidopsis thaliana* reference genome. *Plant Journal* 89:789–804. doi:10.1111/tpj.13415.

Cherry, JM, Hong EL, Amundsen C, Balakrishnan R, Binkley G, Chan ET, Christie KR, Costanzo MC, Dwight SS, Engel SR, Fisk DG, Hirschman JE, Hitz BC, Karra K, Krieger CJ, Miyasato SR, Nash RS, Park J, Skrzypek MS, Simison M, Weng S, Wong ED. 2012. Saccharomyces Genome Database: the genomics resource of budding yeast. *Nucleic Acids Research* 40:D700–D705. doi:10.1093/nar/gkr1029.

Engel SR, Dietrich FS, Fisk DG, Binkley G, Balakrishnan R, Costanzo MC, Dwight SS, Hitz BC, Karra K, Nash RS, Weng S, Wong ED, Lloyd P, Skrzypek MS, Miyasato SR, Simison M, Cherry JM. 2014. The reference genome sequence of Saccharomyces cerevisiae: then and now. *G3: Genes, Genomes, Genetics* 4:389–398. doi:10.1534/g3.113.008995.

Fujiwara M, Uemura T, Ebine K, Nishimori Y, Ueda T, Nakano A, Sato MH, Fukao Y. 2014. Interactomics of Qa-SNARE in *Arabidopsis thaliana*. *Plant and Cell Physiology* 55:781–789. doi:10.1093/pcp/pcu038.

Gallagher CA, Chudzinska M, Larsen-Gray A, Pollock CJ, Sells SN, White PJC, Berger U. 2021. From theory to practice in pattern-oriented modelling: identifying and using empirical patterns in predictive models. *Biological Reviews* 96:1868–1888. doi:10.1111/brv.12729.

Gao XQ, Li CG, Wei PC, Zhang XY, Chen J, Wang XC. 2005. The dynamic changes of tonoplasts in guard cells are important for stomatal movement in *Vicia faba*. *Plant Physiology* 139:1207–1216. doi:10.1104/pp.105.067520.

Gao XQ, Wang XL, Ren F, Chen J, Wang XC. 2009. Dynamics of vacuoles and actin filaments in guard cells and their roles in stomatal movement. *Plant, Cell and Environment* 32:1108–1116. doi:10.1111/j.1365-3040.2009.01993.x.

Glen G, Isaacs K. 2012. Estimating Sobol sensitivity indices using correlations. *Environmental Modelling and Software* 37:157–166. doi:10.1016/j.envsoft.2012.03.014.

Grimm V, Revilla E, Berger U, Jeltsch F, Mooij WM, Railsback SF, Thulke HH, Weiner J, Wiegand T, DeAngelis DL. 2005. Pattern-oriented modeling of agent-based complex systems: lessons from ecology. *Science* 310:987–991. doi:10.1126/science.1116681.

Hetherington AM, Woodward FI. 2003. The role of stomata in sensing and driving environmental change. *Nature* 424:901–908. doi:10.1038/nature01843.

Hills A, Chen ZH, Amtmann A, Blatt MR, Lew VL. 2012. OnGuard, a computational platform for quantitative kinetic modeling of guard cell physiology. *Plant Physiology* 159:1026–1042. doi:10.1104/pp.112.197244.

Hsu PK, Dubeaux G, Takahashi Y, Schroeder JI. 2021. Signaling mechanisms in abscisic acid-mediated stomatal closure. *Plant Journal* 105:307–321. doi:10.1111/tpj.15067.

Järvenpää M, Abdul Sater MR, Lagoudas GK, Blainey PC, Miller LG, McKinnell JA, Huang SS, Grad YH, Marttinen P. 2019. A Bayesian model of acquisition and clearance of bacterial colonization incorporating within-host variation. *PLoS Computational Biology* 15:e1006534. doi:10.1371/journal.pcbi.1006534.

Johnston ST, Simpson MJ, McElwain DL, Binder BJ, Ross JV. 2014. Interpreting scratch assays using pair density dynamics and approximate Bayesian computation. *Open Biology* 4:140097. doi:10.1098/rsob.140097.

Jun Y, Wickner W. 2019. Sec17 (α-SNAP) and Sec18 (NSF) restrict membrane fusion to R-SNAREs, Q-SNAREs, and SM proteins from identical compartments. *Proceedings of the National Academy of Sciences of the United States of America* 116:23573–23581. doi:10.1073/pnas.1913985116.

Kwak JM, Mäser P, Schroeder JI. 2008. The Clickable Guard Cell, version II: interactive model of guard cell signal transduction mechanisms and pathways. *The Arabidopsis Book* 6:e0114. doi:10.1199/tab.0114.

Li LJ, Ren F, Gao XQ, Wei PC, Wang XC. 2013. The reorganization of actin filaments is required for vacuolar fusion of guard cells during stomatal opening in *Arabidopsis*. *Plant, Cell and Environment* 36:484–497. doi:10.1111/j.1365-3040.2012.02592.x.

Liu, F, Li JP, Li LS, Liu Q, Li SW, Song ML, Li S, Zhang Y. 2021. The canonical α-SNAP Is essential for gametophytic development in *Arabidopsis*. *PLoS Genetics* 17:e1009505. doi:10.1371/journal.pgen.1009505.

Mima J, Hickey CM, Xu H, Jun Y, Wickner W. 2008. Reconstituted membrane fusion requires regulatory lipids, SNAREs and synergistic SNARE chaperones. *EMBO Journal* 27:2031–2042. doi:10.1038/emboj.2008.139.

Pandey S, Wang RS, Wilson L, Li S, Zhao Z, Gookin TE, Assmann SM, Albert R. 2010. Boolean modeling of transcriptome data reveals novel modes of heterotrimeric G-protein action. *Molecular Systems Biology* 6:372. doi:10.1038/msb.2010.28.

Reaves BJ, Bright NA, Mullock BM, Luzio JP. 1996. The effect of wortmannin on the localisation of lysosomal type I integral membrane glycoproteins suggests a role for phosphoinositide 3-kinase activity in regulating membrane traffic late in the endocytic pathway. *Journal of Cell Science* 109:749–762. doi:10.1242/jcs.109.4.749.

Ross RJH, Baker RE, Andrew P, Ford MJ, Mort RL, Yates CA. 2017. Using approximate Bayesian computation to quantify cell–cell adhesion parameters in a cell migratory process. *Systems Biology and Applications* 3:9. doi:10.1038/s41540-017-0010-7.

Schäffer AA, Aravind L, Madden TL, Shavirin S, Spouge JL, Wolf YI, Koonin EV, Altschul SF. 2001. Improving the accuracy of PSI-BLAST protein database searches with composition-based statistics and other refinements. *Nucleic Acids Research* 29:2994–3005. doi:10.1093/nar/29.14.2994.

Schroeder JI, Schmidt C, Sheaffer J. 1993. Identification of high-affinity slow anion channel blockers and evidence for stomatal regulation by slow anion channels in guard cells. *Plant Cell* 5:1831–1841. doi:10.2307/3869698.

Schwartz ML, Nickerson DP, Lobingier BT, Plemel RL, Duan M, Angers CG, Zick M, Merz AJ. 2017. Sec17 (α-SNAP) and an SM-tethering complex regulate the outcome of SNARE Zippering *in vitro* and *in vivo*. *ELife* 6:e27396. doi:10.7554/eLife.27396.

Shimazaki KI, Doi M, Assmann SM, Kinoshita T. 2007. Light regulation of stomatal movement. *Annual Review of Plant Biology* 58:219–247. doi:10.1146/annurev.arplant.57.032905.105434.

Song H, Orr A, Duan M, Merz AJ, Wickner W. 2017. Sec17/Sec18 act twice, enhancing membrane fusion and then disassembling cis-SNARE complexes. *ELife* 6:e26646. doi:10.7554/eLife.26646.

Song H, Torng TL, Orr AS, Brunger AT, Wickner WT. 2021. Sec17/Sec18 can support membrane fusion without help from completion of SNARE zippering. *ELife* 10:e67578. doi:10.7554/elife.67578.

Song H, Wickner W. 2019. Tethering guides fusion-competent *trans*-SNARE assembly. *Proceedings of the National Academy of Sciences of the United States of America* 116:13952–13957. doi:10.1073/pnas.1907640116.

Song H, Wickner W. 2021. Fusion of tethered membranes can be driven by Sec18/NSF and Sec17/αSNAP without HOPS. *ELife* 10:e73240. doi:10.7554/eLife.73240.

Starai VJ, Hickey CM, Wickner W. 2008. HOPS proofreads the *trans*-SNARE complex for yeast vacuole fusion. *Molecular Biology of the Cell* 19:2500–2508. doi:10.1091/mbc.E08–01–0077.

Takemoto K, Ebine K, Askani JC, Krüger F, Gonzalez ZA, Ito E, Goh T, Schumacher K, Nakano A, Ueda T. 2018. Distinct sets of tethering complexes, SNARE complexes, and Rab GTPases mediate membrane fusion at the vacuole in *Arabidopsis*. *Proceedings of the National Academy of Sciences of the United States of America* 115:E2457–E2466. doi:10.1073/pnas.1717839115.

Toni T, Welch D, Strelkowa N, Ipsen A, Stumpf MPH. 2009. Approximate Bayesian computation scheme for parameter inference and model selection in dynamical systems. *Journal of the Royal Society Interface* 6:187–202. doi:10.1098/rsif.2008.0172.

Ungermann C, Sato K, Wickner W. 1998. Defining the functions of *trans*-SNARE Pairs. *Nature* 396:543–548. doi:10.1038/25069.

Vialet-Chabrand S, Hills A, Wang Y, Griffiths H, Lew VL, Lawson T, Blatt MR, Rogers S. 2017. Global sensitivity analysis of OnGuard models identifies key hubs for transport interaction in stomatal dynamics. *Plant Physiology* 174:680–688. doi:10.1104/pp.17.00170.

Waese J, Fan J, Pasha A, Yu H, Fucile G, Shi R, Cumming M, Kelley LA, Sternberg MJ, Krishnakumar V, Ferlanti E, Miller J, Town C, Stuerzlinger W, Provart NJ. 2017. EPlant: visualizing and exploring multiple levels of data for hypothesis generation in plant biology. *Plant Cell* 29:1806–1821. doi:10.1105/tpc.17.00073.

Wang M, White N, Grimm V, Hofman H, Doley D, Thorp G, Cribb B, Wherritt E, Han L, Wilkie J, Hanan J. 2018. Pattern-oriented modelling as a novel way to verify and validate functional-structural plant models: a demonstration with the annual growth module of avocado. *Annals of Botany* 121:941–959. doi:10.1093/aob/mcx187.

Wang M, White N, Hanan J, He D, Wang E, Cribb B, Kriticos DJ, Paini D, Grimm V. 2020. Parameter estimation for functional-structural plant models when data are scarce: using multiple patterns for rejecting unsuitable parameter sets. *Annals of Botany* 126:559–570. doi:10.1093/aob/mcaa016.

Wickner W. 2010. Membrane fusion: five lipids, four SNAREs, three chaperones, two nucleotides, and a Rab, all dancing in a ring on yeast vacuoles. *Annual Review of Cell and Developmental Biology* 26:115–136. doi:10.1146/annurev-cellbio-100109-104131.

Wiegand T, Jeltsch F, Hanski I, Grimm V. 2003. Using pattern-oriented modeling for revealing hidden information: a key for reconciling ecological theory and application. *OIKOS* 100:209–222. doi:10.1034/j.1600-0706.2003.12027.x.

Woolfenden HC, Bourdais G, Kopischke M, Miedes E, Molina A, Robatzek S, Morris RJ. 2017. A computational approach for inferring the cell wall properties that govern guard cell dynamics. *Plant Journal* 92:5–18. doi:10.1111/tpj.13640.

Xu H, Jun Y, Thompson J, Yates J, Wickner W. 2010. HOPS prevents the disassembly of *trans*-SNARE complexes by Sec17p/Sec18p during membrane fusion. *EMBO Journal* 29:1948–1960. doi:10.1038/emboj.2010.97.

Zheng J, Han SW, Rodriguez-Welsh MF, Rojas-Pierce M. 2014. Homotypic vacuole fusion requires VTI11 and is regulated by phosphoinositides. *Molecular Plant* 7:1026–1040. doi:10.1093/mp/ssu019.

Zick M, Orr A, Schwartz ML, Merz AJ, Wickner WT. 2015. Sec17 can trigger fusion of *trans*-SNARE paired membranes without Sec18. *Proceedings of the National Academy of Sciences of the United States of America* 112:E2290–E2297. doi:10.1073/pnas.1506409112.

Zick M, Wickner W. 2013. The tethering complex HOPS catalyzes assembly of the soluble SNARE Vam7 into fusogenic *trans*-SNARE complexes. *Molecular Biology of the Cell* 24:3746–3753. doi:10.1091/mbc.E13-07-0419.

Ziegler C, Dyson RJ, Johnston IG. 2019. Model selection and parameter estimation for root architecture models using likelihood-free inference. *Journal of the Royal Society Interface* 16:20190293. doi:10.1098/rsif.2019.0293.